Lifetime measurements and nuclear deformation in the $A \approx 100$ region

A. G. Smith, J. L. Durell, W. R. Phillips, and W. Urban*
School of Physics and Astronomy, University of Manchester, Manchester M13 9PL, United Kingdom

P. Sarriguren
Instituto de Estructura de la Materia, IEM-CSIC, Serrano 123, E-28006 Madrid, Spain

I. Ahmad
Argonne National Laboratory, Argonne, Illinois 60439, USA
(Received 25 May 2012; published 19 July 2012)

The EUROGAM-2 array has been used to study γ rays emitted following the spontaneous fission of a ^{248}Cm source. Analysis of Doppler-broadened lineshapes corresponding to transitions from excited rotational states in neutron-rich Sr, Zr, Mo, Ru, and Pd fission fragments has enabled measurements of state lifetimes in these nuclei at nuclear spins of $I \sim 10$. Extracted transition quadrupole moments are compared with various recent theoretical approaches, as well as with measurements at lower spin, and an interpretation of the data is made within the context of prolate-oblate shape competition in this region.

DOI: 10.1103/PhysRevC.86.014321 PACS number(s): 27.60.+j, 21.10.Dr, 23.20.Lv, 21.10.Ft

I. INTRODUCTION

Atomic nuclei are known to exhibit a variety of shapes whose deviation from sphericity can be well described as combinations of quadrupole and higher-order multipole deformations. Quadrupole deformations are the most common and may be expressed in terms of the parameters β_2 and γ [1]. Axially symmetric prolate deformations with the rotation axis perpendicular to the symmetry axis correspond to $\gamma = 0$, while $\gamma = +60^\circ$ describes an axially symmetric oblate shape and $\gamma = 30^\circ$ describes a maximally triaxial nucleus. The shape that a particular nucleus takes up results from a delicate balance between the collective (macroscopic) and single-particle (microscopic) energies and is therefore dependent on both the atomic number Z and the neutron number N. Also, because nuclear rotation perturbs the microscopic structure of the nucleus, it may be that the shapes favoured by a particular nucleus will change with the nuclear spin I [2,3]. This threefold sensitivity of the nuclear shape to Z, N, and I provides a severe test of current theoretical approaches to low-energy nuclear structure. The neutron-rich strontium, zirconium, molybdenum, ruthenium, and palladium nuclei provide fertile territory for the exploration of this three-fold sensitivity. It has been established that, as the neutron number is increased from the valley of stability, the onset of quadrupole deformation occurs [4–6]. The transition from a spherical to a deformed ground state is sudden for Sr and Zr isotopes, but is more gradual for higher-Z nuclei. Furthermore, increasing proton number from $Z = 40$ has the effect of softening the nuclear energy surface to triaxiality, evidence for which comes from a variety of sources, namely: the observation in ^{106}Mo of a two-phonon vibrational state [7], which shows that ^{106}Mo is soft to triaxial deformation; the identification of the energy levels of the neutron-rich even-A Ru isotopes [8–10] with the rotation of a rigid triaxial rotor; the rotational levels and branching ratios of the odd-A Mo isotopes [11] and the g factors of excited states in ^{105}Mo [12], both of which have been interpreted within the context of a triaxial particle-rotor model with static nonzero γ deformation; the recent measurement of the decay scheme of the nucleus ^{110}Mo [13] and interpretation in terms of axial asymmetry [14]; the identification of mixed oblate-prolate yrast states [15] and low-lying oblate states [16] in ^{111}Tc; and finally, the observation of a possible oblate isomer in ^{109}Nb [17].

The measurement of the mean lifetimes of rotational states provides the means to probe the nuclear shape at intermediate to high spin, since the electric quadrupole transition matrix elements in a rotational band are simply related to the magnitude of the quadrupole deformation of the intrinsic nuclear state. Before the advent of large arrays of high-purity Ge detectors, most of the experimental information on the shapes of the neutron-rich nuclei near $Z = 40$ had been limited to low spins. The development of the Doppler profile method (DPM) [18] resulted in the publication of the results of lifetime analyses in ^{98}Sr, ^{100,102,104}Zr and ^{102,104,106,108}Mo [19], and ^{96,97,100}Sr, ^{98,99}Zr [20]. These results are reproduced here in Tables I–III. In this paper we report additional lifetime measurements for ^{101}Zr, ^{103}Nb, ^{103,105,107}Mo, ^{108,109,110,111,112}Ru, and ^{114,116}Pd, and use the whole set of results, including the previously published data, as a basis for the discussion of the evolution of nuclear shape in the $A \sim 100$ region from $_{38}$Sr to $_{46}$Pd.

II. EXPERIMENTAL DETAILS AND ANALYSIS TECHNIQUES

In this work the spontaneously fissioning nuclide ^{248}Cm was used as a source of neutron-rich fission fragments whose electromagnetic decay properties were to be studied. The

*Present addresses: Institut Laue-Langevin, B.P. 156, F-38042 Grenoble Cedex 9, France and Faculty of Physics, University of Warsaw, ul.Hoża 69, PL-00-681 Warszawa, Poland.

TABLE I. The quadrupole moments and lifetimes deduced from our lineshape analysis for states in ^{96,97,98,100}Sr and ^{98,99,100}Zr. Also listed are the spin and γ-ray decay energy for each state used in the decay simulation. The errors quoted for $Q_{\rm DPM}$ are purely statistical in origin and a further systematic error of 5% exists due to uncertainties in the stopping powers. The DPM lifetimes are computed from $Q_{\rm DPM}$ and within any one band do not represent independent measurements. The first error on the lifetime represents the statistical uncertainty in the measurement and the second is a result of a 10% uncertainty in the stopping powers.

Nucleus	Ref. [68]	Ref. [69]	DPM results			
Config.	Q_{2^+} [eb]	Q_0 [eb]	$Q_{\rm DPM}$ [eb]	E_γ [keV]	$I_i \rightarrow I_f$	τ [ps]
$^{96}_{38}$Sr$_{58}$	1.48(48)	2.93	2.10(10)	838.5	12 → 10	1.30(12)(13)
yrast				761.0	10 → 8	2.16(20)(22)
				659.4	8 → 6	4.54(44)(45)
$^{97}_{38}$Sr$_{59}$		3.05	2.90(20)	774.0	27/2 → 23/2	1.18(16)(12)
$K^\pi = \frac{3}{2}^-, \alpha = -\frac{1}{2}$				653.5	23/2 → 19/2	2.87(40)(29)
$^{98}_{38}$Sr$_{60}$	3.59(05)	3.14	3.17(19)	812.5	12 → 10	0.67(08)(07)
yrast				689.4	10 → 8	1.55(19)(15)
				565.7	8 → 6	4.28(54)(43)
$^{100}_{38}$Sr$_{62}$	3.78(11)	3.28	3.70(21)	689.8	10 → 8	1.15(14)(11)
yrast				566.3	8 → 6	3.08(34)(30)
$^{98}_{40}$Zr$_{58}$		3.06	2.10(23)	769.8	10 → 8	2.05(44)(20)
yrast (0^+ band)				725.7	8 → 6	2.82(62)(28)
$^{99}_{40}$Zr$_{59}$		3.26	2.60(12)	714.1	23/2 → 19/2	2.30(22)(23)
$K^\pi = \frac{3}{2}^-, \alpha = -\frac{1}{2}$				566.0	19/2 → 15/2	7.83(72)(78)
$^{100}_{40}$Zr$_{60}$	3.34(9)	3.36	3.19(10)	841.7	12 → 10	0.54(03)(05)
yrast				739.2	10 → 8	1.08(06)(10)
				625.6	8 → 6	2.55(17)(25)

source consisted of about 5 mg of curium oxide (giving a fission rate of about 7×10^4 per second) embedded in a pellet of potassium chloride. The pellet was large enough (0.5 mm thick and 5 mm in diameter) that the fission fragments were stopped within it. The EUROGAM phase 2 array [21] of Compton-suppressed germanium detectors was used to detect the γ rays emitted in the decay of the excited fission fragments. Around 2.5×10^9 coincidence events with more than three γ rays were recorded on magnetic tape. From these data a $\gamma\gamma\gamma$ cube and a $\gamma\gamma\gamma\gamma$ hypercube [22] were constructed. To obtain spectra that emphasized a particular decay sequence triple-gated 1D spectra from the hypercube were used, though in a few cases where the statistics were very poor, double-gated 1D spectra from the cube were also required. At spins of $I \sim 10$, symmetrically Doppler-broadened lineshapes are observed in the γ-ray energy spectra of many of the rotational bands in the light fission fragments. The broad lineshapes correspond to transitions from states that have lifetimes comparable to

TABLE II. The quadrupole moments and lifetimes deduced from our lineshape analysis for states in ^{101,102,104}Zr and ^{103}Nb. Also listed are the spin and γ-ray decay energy for each state used in the decay simulation. The errors quoted for $Q_{\rm DPM}$ are purely statistical in origin and a further systematic error of 5% exists due to uncertainties in the stopping powers. The DPM lifetimes are computed from $Q_{\rm DPM}$ and within any one band do not represent independent measurements. The first error on the lifetime represents the statistical uncertainty in the measurement and the second is a result of a 10% uncertainty in the stopping powers.

Nucleus	Ref. [68]	Ref. [69]	DPM results			
Config.	Q_{2^+} [eb]	Q_0 [eb]	$Q_{\rm DPM}$ [eb]	E_γ [keV]	$I_i \rightarrow I_f$	τ [ps]
$^{101}_{40}$Zr$_{61}$		3.48	3.92(30)	712.0	23/2 → 19/2	0.95(15)(09)
5/2[532]				569.4	19/2 → 15/2	3.14(48)(31)
$^{101}_{40}$Zr$_{61}$			3.60(20)	696.0	21/2 → 17/2	1.26(14)(13)
3/2[411]				578.3	17/2 → 13/2	3.44(38)(34)
$^{102}_{40}$Zr$_{62}$	4.06(42)	3.51	3.52(17)	860.8	12 → 10	0.40(05)(04)
yrast				756.6	10 → 8	0.77(09)(08)
				630.1	8 → 6	2.01(23)(20)
$^{104}_{40}$Zr$_{64}$		3.68	3.72(16)	894.4	12 → 10	0.29(03)(03)
yrast				765.1	10 → 8	0.67(07)(07)
				624.4	8 → 6	1.91(21)(20)
$^{103}_{41}$Nb$_{62}$		3.82	3.60(20)	729.8	21/2 → 17/2	1.03(11)(10)
5/2[303]				618.3	17/2 → 13/2	2.62(29)(26)

TABLE III. The quadrupole moments and lifetimes deduced from our lineshape analysis for states in ^{102,103,104,105,106,107,108}Mo and ^{108,109}Ru. Also listed are the spin and γ-ray decay energy for each state used in the decay simulation. The errors quoted for $Q_{\rm DPM}$ are purely statistical in origin and a further systematic error of 5% exists due to uncertainties in the stopping powers. The DPM lifetimes are computed from $Q_{\rm DPM}$ and within any one band do not represent independent measurements. The first error on the lifetime represents the statistical uncertainty in the measurement and the second is a result of a 10% uncertainty in the stopping powers.

Nucleus	Ref. [68]	Ref. [69]	DPM results			
Config.	Q_{2^+} [eb]	Q_0 [eb]	$Q_{\rm DPM}$ [eb]	E_γ [keV]	$I_i \rightarrow I_f$	τ [ps]
$^{102}_{42}$Mo$_{60}$	3.11(05)	3.29	2.44(17)	834.9	$12 \rightarrow 10$	0.95(13)(10)
yrast				771.5	$10 \rightarrow 8$	1.49(21)(15)
				690.9	$8 \rightarrow 6$	2.66(37)(27)
$^{103}_{42}$Mo$_{61}$		3.60	3.10(20)	706.8	$23/2 \rightarrow 19/2$	1.58(20)(16)
5/2[532]				547.1	$19/2 \rightarrow 15/2$	6.13(79)(61)
$^{104}_{42}$Mo$_{62}$	3.67(11)	3.54	2.84(14)	733.6	$10 \rightarrow 8$	1.42(14)(14)
yrast				641.8	$8 \rightarrow 6$	2.84(31)(28)
$^{105}_{42}$Mo$_{63}$		3.76	3.50(20)	693.5	$23/2 \rightarrow 19/2$	1.36(16)(14)
5/2[532]				556.7	$19/2 \rightarrow 15/2$	4.39(50)(44)
$^{106}_{42}$Mo$_{64}$	3.63(10)	3.70	2.85(13)	896.7	$12 \rightarrow 10$	0.53(05)(05)
yrast				784.1	$10 \rightarrow 8$	1.00(09)(10)
				654.9	$8 \rightarrow 6$	2.55(23)(26)
$^{107}_{42}$Mo$_{65}$		3.63	3.45(20)	698.7	$23/2 \rightarrow 19/2$	1.35(16)(14)
7/2[523]				557.5	$19/2 \rightarrow 15/2$	4.50(52)(45)
$^{108}_{42}$Mo$_{66}$	4.0(6)	3.46	2.79(20)	867.1	$12 \rightarrow 10$	0.63(09)(06)
yrast				776.6	$10 \rightarrow 8$	1.11(16)(11)
				662.1	$8 \rightarrow 6$	2.52(36)(25)
$^{108}_{44}$Ru$_{64}$	3.18(24)	3.06	2.46(20)	787.8	$12 \rightarrow 10$	1.29(20)(13)
(Yrast)				798.3	$10 \rightarrow 8$	1.25(20)(13)
				701.6	$8 \rightarrow 6$	2.43(39)(24)
$^{109}_{44}$Ru$_{65}$		3.21	2.84(15)	828	$27/2 \rightarrow 23/2$	0.81(9)(8)
5/2[532]				691.5	$23/2 \rightarrow 19/2$	2.09(23)(21)

(or faster than) the stopping time (1–2 ps) of the fission fragments in the source pellet, the broadening being due to the variable Doppler-shift that is observed for the time distribution of transitions from such states. In general, there are several possibilities for gating on a given band; in choosing the gating transitions we have tried to place one gate on transitions that precede the transitions of interest, so as to exclude the effect of side-feeding (see below). These gates on the preceding transitions are necessarily wide in order not to bias the velocity distribution of the fission fragments, and are only possible through the use of triple-gated spectra in which two narrow gates are placed lower in the band to cleanly select the decay sequence, on γ-ray transitions that are emitted after the states being fitted have decayed.

The DPM combines a simulation of the stopping of the isotropically directed fission fragment with a simulation of the electromagnetic decay to generate a lineshape that can be compared directly with the data and thereby extract state lifetimes. The stopping of the fragment in the KCl pellet is simulated with a Monte Carlo computer code using electronic and nuclear stopping powers given by the computer code ZBL [23]. The initial fragment kinetic energy distribution was assumed to be Gaussian with its centroid taken from [24] (with a Coulomb correction for the particular charge split) and width taken to be the same as that measured for the light fragments from ^{252}Cf spontaneous fission [25]. The simulation produced a two-dimensional data matrix (fractional Doppler shift, or FDS matrix) whose contents gave the probability of observing a particular fractional Doppler shift ($\beta \cos\theta$, where β is the velocity of the fragment and θ is the angle between the fragment velocity and the γ-ray detection axis) in the emitted radiation at any given time. Anisotropic angular distributions of the γ radiation relative to the fragment velocity direction can, in principle, affect the form of the FDS matrix but these effects are relatively small in fission and have been neglected in the present analysis.

In modeling the electromagnetic decay of the excited fission fragment, consideration must be given to the time distribution of the intensity feeding the states whose lifetimes are to be determined. For the highest-spin state whose decay produces an observed lineshape it is not possible to extract any information directly from the γ-ray spectrum about the feeding distribution, so the feeding of this state is simulated by a two-state feeding model in which the lifetimes of both feeding states are varied in the fit. For all other states there is some information regarding the feeding distribution contained in the lineshape of the decay into the state, although a large fraction (40–60%) of the population of the state is provided by unobserved "side-feeding" transitions. Measurements of γ-ray multiplicities following spontaneous fission suggest that a yrast state at intermediate spin is fed predominantly by a combination of fast statistical γ rays, and the transition from the next-highest spin yrast state. Although slow side-feeding components have been observed they constitute typically a few

percent of the decay intensity. In the present analysis, in cases where side-feeding could not be eliminated through a clean gate above[1] the state of interest it was necessary to include a model for the time distribution of the unobserved contribution to the population of the state. This distribution was simulated in the fitting procedure by a two-state model with a variable feeding time. To reduce the effect of possible contamination of the lineshapes with sharp lines from the heavy fragments and to improve the stability of the fit, the rotational band was assumed to correspond to the rotation of a nucleus of constant intrinsic quadrupole moment (Q). Within this model, the mean lifetime (τ in ps) of a state of spin I, decaying within a rotational band by a stretched $E2$ γ ray of energy E_γ (in MeV) is given by

$$\frac{1}{\tau} \approx 1.217\langle I, K, 2, 0|I-2, K\rangle^2 Q^2 E_\gamma^5,$$

where $\langle I, K, 2, 0|I-2, K\rangle$ is a Clebsch-Gordan coefficient and Q is measured in e barns (eb). Q was used to vary the state lifetimes in a manner consistent with this assumption, the best fit to the data resulting in a solution we label as $Q_{\rm DPM}$. Although Q may vary somewhat with spin, this procedure gives the most consistent treatment of the data. Nevertheless, it should be borne in mind that the value of $Q_{\rm DPM}$ extracted in this analysis represents an effective quadrupole moment over three or four states at around $I \sim 10$. The quantum number K represents the projection of the intrinsic angular momentum on the symmetry axis. Strictly speaking, it is well defined only in the case of axially symmetric nuclei at low rotational frequencies and large deformations. In all even-nuclei examined here, K was taken as zero, whereas for the odd nuclei the bandhead value of K was used. Since it is usually difficult to determine the centroid energy of the Doppler-broadened lineshapes to a level of accuracy comparable to experiments that produce narrow lineshapes, we have consistently used the evaluated γ-ray energies [26–41] in our fits and calculations of the state lifetimes. Examples of Doppler-broadened lineshapes for the $I^\pi = 10^+ \rightarrow 8^+$ transitions in the yrast bands of ^{100}Zr and ^{108}Mo, with the corresponding best fits are shown in Fig. 1.

III. RESULTS OF LINESHAPE ANALYSIS

A. ^{101}Zr

Previous data on the yrast states populated in spontaneous fission have been reported in Ref. [42] in which rotational bands based on the 3/2[411], 9/2[404], and 5/2[532] neutron Nilsson states were observed. Doppler-broadened lineshapes were observed for the 712.0 keV and 569.4 keV transitions in the 5/2[532] band and the 696.0 keV and 578.3 keV transitions in the 3/2[411] band. The resulting quadrupole moments and deduced lifetimes are presented in Table II.

[1]We use the terms *above* and *below* as a shorthand to indicate whether a transition precedes or follows, respectively, the transition of interest in the time-order of a decay sequence.

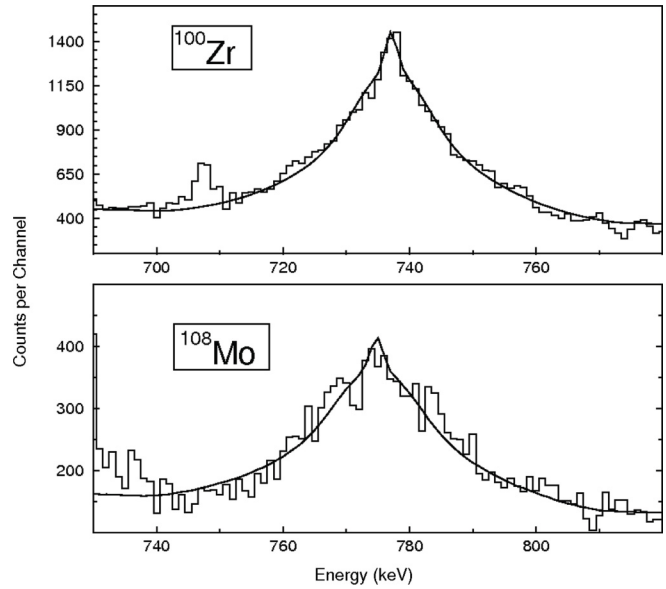

FIG. 1. Examples of fitted lineshapes in ^{100}Zr and ^{108}Mo for the $I = 10 \rightarrow 8$ transitions (see Tables I and III for the resulting transition quadrupole moments).

B. ^{103}Nb

Rotational bands built on the proton 5/4[422], the 5/2[303] and the 3/2[301] Nilsson states have been observed in previous work [6,43–46]. Doppler broadened lineshapes have been observed in this experiment for the 729.6 keV and 618.3 keV transitions in the 5/2[303] band. The resulting quadrupole moment and deduced lifetimes are presented in Table II.

C. ^{103,105,107}Mo

The ^{103}Mo nucleus has been previously studied following the β^- decay of ^{103}Nb [47] and after population in spontaneous fission [6,44,48,49]. In this work, Doppler-broadened lineshapes have been observed for the 706.8 keVand 547.1 keV transitions in the 5/2[532] band. ^{105}Mo has been previously studied in the β^- decay of ^{105}Nb [50] and in spontaneous fission [6,44,49,51]. In this work the Doppler-broadened lines are the 693.5 keV and the 556.7 keV transitions from the band built on the 5/2[532] intrinsic neutron state. ^{107}Mo has been studied previously in spontaneous fission of a ^{248}Cm source with EUROGAM [52] (the same data set used in the present paper), and with mass separated fission fragments at Lohengrin [11]. From these experiments rotational bands have been observed built on the 7/2[523], 3/2[411] and 5/2[413] intrinsic states. In this experiment, broadened lineshapes were observed for the 698.7 keV and 557.5 keV transitions in the rotational band built on the 7/2[523] intrinsic neutron state. The resulting quadrupole moments and deduced lifetimes are presented in Table III.

D. ^{108,109,110,111,112}Ru

^{108}Ru has been previously observed in the β^- decay of ^{108}Tc [53], in the spontaneous fission of ^{252}Cf [54] and in

TABLE IV. The quadrupole moments and lifetimes deduced from our lineshape analysis for states in ^{110,111,112}Ru and ^{1114,116}Pd. Also listed are the spin and γ-ray decay energy for each state used in the decay simulation. The errors quoted for Q_{DPM} are purely statistical in origin and a further systematic error of 5% exists due to uncertainties in the stopping powers. The DPM lifetimes are computed from Q_{DPM} and within any one band do not represent independent measurements. The first error on the lifetime represents the statistical uncertainty in the measurement and the second is a result of a 10% uncertainty in the stopping powers.

Nucleus	Ref. [68]	Ref. [69]	DPM results			
Config.	Q_{2^+} [eb]	Q_0 [eb]	Q_{DPM} [eb]	E_γ [keV]	$I_i \rightarrow I_f$	τ [ps]
$^{110}_{44}Ru_{66}$	3.24(19)	2.75	2.60(30)	814.7	$10 \rightarrow 8$	1.00(12)(10)
(Yrast)				705.7	$8 \rightarrow 6$	2.11(25)(21)
$^{111}_{44}Ru_{67}$		2.86	3.06(15)	846.0	$31/2 \rightarrow 27/2$	0.60(6)(6)
$K^\pi = \frac{7}{2}^-$				760.7	$27/2 \rightarrow 23/2$	1.06(11)(11)
				650.9	$23/2 \rightarrow 19/2$	2.42(24)(24)
$^{112}_{44}Ru_{68}$	3.41(34)	2.88	2.85(15)	763.1	$12 \rightarrow 10$	1.15(13)(12)
(Yrast)				722.6	$10 \rightarrow 8$	1.52(17)(15)
				649.7	$8 \rightarrow 6$	2.65(29)(27)
$^{112}_{44}Ru_{68}$			2.95(15)	756.0	$11 \rightarrow 9$	1.12(11)(11)
($\alpha = 1$)				693.8	$9 \rightarrow 7$	1.77(18)(18)
				605.3	$7 \rightarrow 5$	3.60(36)(36)
$^{114}_{46}Pd_{68}$	1.93(31)	2.94	2.92(21)	864.3	$16 \rightarrow 14$	0.65(09)(07)
(Yrast)				704.1	$14 \rightarrow 12$	1.52(20)(15)
$^{116}_{46}Pd_{70}$	2.47(37)	3.02	1.81(23)	849.7	$16 \rightarrow 14$	1.65(36)(17)
(Yrast)			2.80(20)	710.6	$14 \rightarrow 12$	1.67(24)(17)

a heavy-ion fusion-fission experiment with a ^{28}Si beam on a target of ^{176}Yb [55]. These investigations resulted in the determination of the yrast levels to a spin of $I = 16$. In the present work, lineshapes have been analyzed for the 701.6, the 798.3, and the 787.8 keV transitions in the yrast band, and the resulting transition quadrupole moments and associated lifetimes shown in Table III.

^{109}Ru has been previously studied in the β^- decay of ^{109}Tc [56] and through fission of ^{252}Cf sources [57–59]. The level-scheme deduced in these earlier papers extends to a spin of $I = 27/2$. More recently, the level scheme has been extended [9] to $I = 39/2$ and the γ-ray transitions used for lineshape analysis in the present paper are the 691.5 and 822 keV transitions as identified in that work. The resulting transition quadrupole measurements and associated state lifetimes are presented in Table III.

^{110}Ru has been previously studied following β^- decay of mass-separated ^{110}Tc [60] and in the spontaneous fission of ^{252}Cf [10,54,61] and of ^{248}Cm [8]. In the present work Doppler-broadened lineshapes for the 814.7 keV and 705.7 keV transitions of the yrast sequence permit lifetime measurements. The nucleus ^{111}Ru has been observed in the β^- decay of mass-separated ^{111}Tc produced in proton-induced fission of uranium [62], and in the spontaneous fission of ^{248}Cm [63] and ^{252}Cf [57]. Rotational bands have been assigned to bandheads with $K^\pi = \frac{5}{2}^+, \frac{1}{2}^+, \frac{7}{2}^-, \frac{11}{2}^-$, and $\frac{9}{2}^-$. Here, lifetime measurements have been performed using the 846.0, 760.7, and 650.9 keV transitions of the band assigned to a $K^\pi = \frac{7}{2}^-$ bandhead. The low spin rotational bands in ^{112}Ru have been observed in ^{112}Tm β^- decay [60] as well as various ion-induced and spontaneous fission reactions (see [39] and references therein) and more recently to higher spin with ^{238}U(α, f) [9]. Of the previously observed transitions in the yrast sequence, Doppler-broadened lineshapes were observed for the 763.0, 722.6, and the 649.7.3 keV lines. In addition, broadened lineshapes have been fitted for the 756.0, 693.8, and 605.3 keV transitions in the $\alpha = 1$ sequence; this corresponds to the γ band, as discussed by Shannon *et al.* [8]. The resulting transition quadrupole moment measurements are presented in Tables III and IV. An example of the lineshapes in ^{112}Ru with the resulting best fit is shown in Fig. 2.

E. ^{114,116}Pd

^{114}Pd has been studied in the β^- decay of mass-separated ^{114}Rh [64], and the low to medium-spin yrast levels

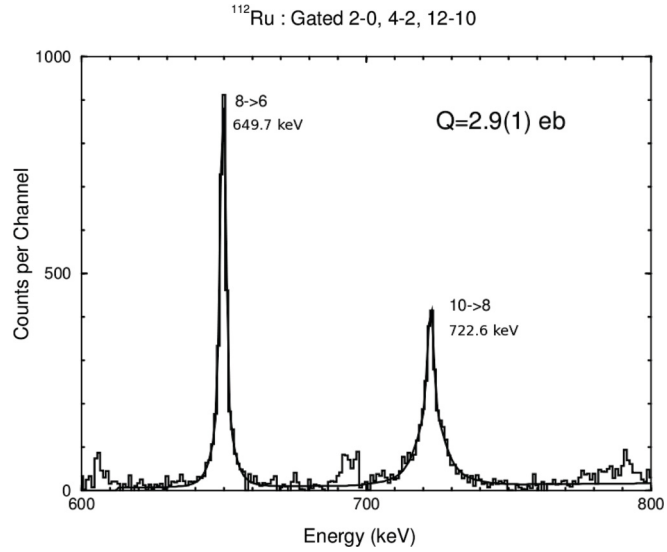

FIG. 2. Fitted lineshapes for ^{112}Ru.

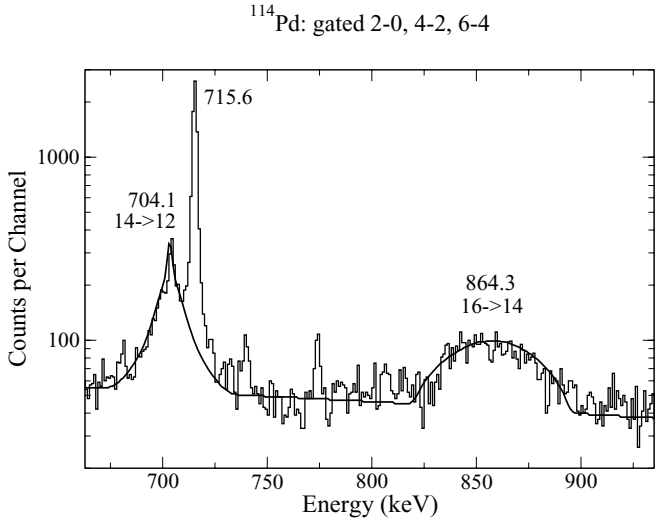

FIG. 3. Fitted lineshapes in ^{114}Pd.

determined in the spontaneous fission of ^{252}Cf [65]. Here, we observed Doppler-broadened γ-ray lineshapes for the 864.3 and 704.1 keV transitions.

^{116}Pd has been observed in the β^- decay of ^{116}Rh [64,66], in the spontaneous fission of ^{252}Cf [65], and in ^{238}U(α, f) [67]. From the analysis of these experiments the low to medium spin level scheme has been established. The yrast sequence is known up to $I = 22$ and in the present work Doppler-broadened lineshapes have been observed for the 849.7 and 710.6 keV lines. Examples of fitted spectra are shown in Figs. 3 and 4 where it may be observed that the $(I=)16 \rightarrow 14$ transitions (864.2 keV in ^{114}Pd and 849.7 keV in ^{116}Pd) have significantly different widths. This is due in part to the difference in transition energy, but to get a good fit requires the use of different quadrupole moments for the $(I=)16 \rightarrow 14$ and $14 \rightarrow 12$ transitions in ^{116}Pd. This is the only case in the analysis of the whole region where the nature of the spectra has forced a departure from the use of the constant-Q approach. In such a case, the lower-spin result should be considered

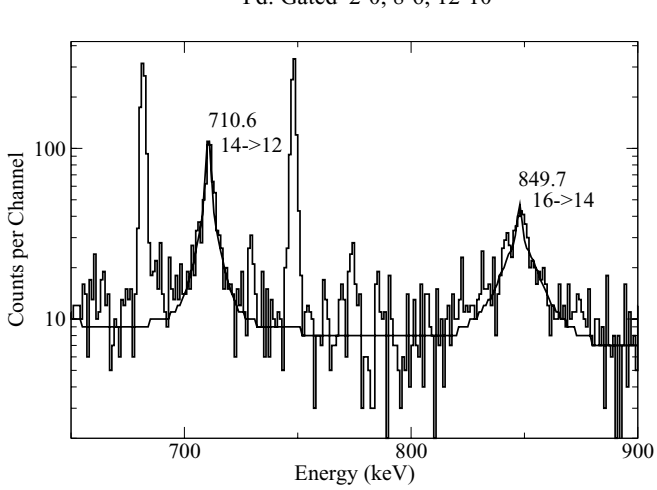

FIG. 4. Lineshapes for the yrast sequence in ^{116}Pd.

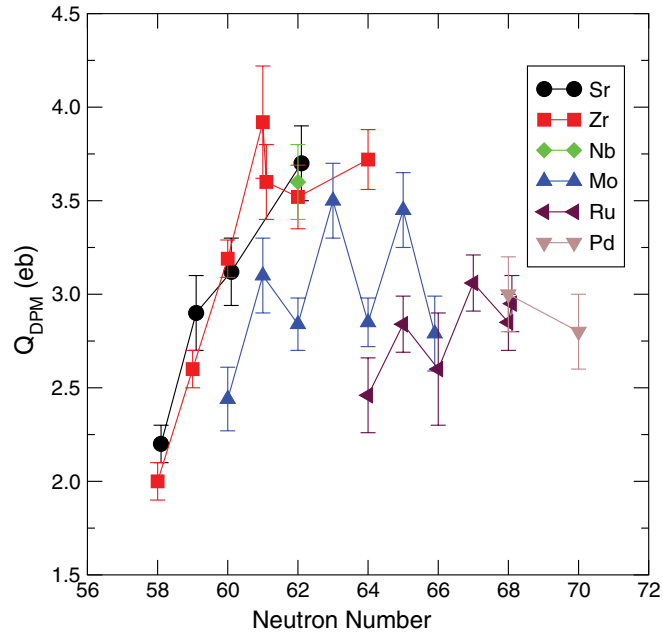

FIG. 5. (Color online) Transition quadrupole moments deduced from the lineshapes of transitions from states with $I \sim 10$ in the mass 100 region.

the more reliable since the time-distribution of the feeding is constrained by the observed shape of the preceding lineshape. The fit to the ^{114}Pd data excludes the contribution of the lower-lying (and hence narrow) 715.6 keV transition from the 8^+ state to the 6^+ state of the ground state band. The resulting transition quadrupole moments and associated lifetimes are listed in Table IV.

IV. DISCUSSION

Figure 5 shows the transition quadrupole moments $Q_{\rm DPM}$ plotted against neutron number for the neutron-rich isotopes of $_{38}$Sr, $_{40}$Zr, $_{41}$Nb, $_{42}$Mo, $_{44}$Ru, and $_{46}$Pd measured in this experiment. The onset of deformation at $N \approx 60$ is clearly seen in the Sr and Zr isotopes with $Q_{\rm DPM}$ rising from around 2.0 eb at $N = 58$ to above 3.5 eb at $N = 62$. As the atomic number is increased, the Mo isotopes also show the onset of deformation, but display evidence of a softer shape with pronounced odd-even staggering; the odd-A isotopes having greater $Q_{\rm DPM}$ than the even-A isotopes by about 0.5 eb. As Z is further increased into the Ru and Pd isotopes there appears to be something of a transition to smaller deformations ($Q_{\rm DPM}$ below 3.0 eb), less-pronounced odd-even staggering and only a gentle increase in quadrupole moment with neutron number from $N = 64$ to $N = 70$. Figure 5 is largely suggestive of there being two distinct groups of nuclei; the Sr and Zr isotopes, with rapidly rising deformation and a high maximum $Q_{\rm DPM}$, and the Ru and Pd isotopes, which are less deformed and show a weak dependence of $Q_{\rm DPM}$ on N. The odd-A Mo isotopes have more of the characteristics of the the Sr and Zr group, while the even-A Mo isotopes behave more akin to the Ru and Pd nuclei.

There now exist a wealth of theoretical calculations of equilibrium shapes in the mass 100 region. Some of the more recent that allow the prediction of quadrupole moments, include: the folded-Yukawa single-particle with finite-range liquid-drop calculations of Möller *et al.* [69]; the cranked Woods-Saxon Nilsson-Strutinsky with monopole residual interaction approach of Skalski *et al.* [70]; and the self-consistent mean-field with D1S-Gogny interaction calculations of Rodriguez-Guzman *et al.* [71,72]. Of these, only the Skalski calculations include the effect of nuclear rotation; the other calculations are explicitly for the ground state. On the other hand, Ref. [70] deals only with even-even nuclei whereas the other works calculate nuclear shapes for odd as well as even particle numbers.

A comparison with Ref. [69] is perhaps instructive in the first instance since these calculations are extremely extensive, including 8979 nuclei and most of the nuclear chart (with the exception of nuclei lighter than ^{16}O) with a coherent theoretical approach that predicts both ground state masses as well as nuclear shapes. As such, it places the $A \sim 100$ region within a broader theoretical perspective. The solutions to the ground-state deformation are published in terms of the β_2, β_3, β_4, and β_6 deformation parameters. In order to make a comparison with $Q_{\rm DPM}$ we have used the conversion to the intrinsic quadrupole moment

$$Q_0 = \sqrt{\frac{16\pi}{5}}\,\frac{3}{4\pi}\,ZeR_0^2\beta_2,$$

where $R_0 = 1.2A^{1/3}$ fm is the nuclear radius. In doing so, we make the assumption that the quadrupole deformation parameters and radii of the mass and charge distributions are identical, and that there is no effect of higher-order multipoles on the transition matrix element in the nuclear decay. The resulting quadrupole moments are listed in Tables I to IV. The upper panel in Fig. 6 shows Q_0 plotted against neutron number for the nuclei measured in this work. In the lower panel of Fig. 6 the difference between Q_0 and $Q_{\rm DPM}$ is plotted as a function of neutron number. The average deviation between theory and experiment over the region is 0.33 eb, i.e., on average the calculated moments are slightly higher than the data, but there are clearly significant systematic differences that are larger than the uncertainties on the data points. The theoretical quadrupole moments of the $N = 58$ Sr and Zr isotones are higher than the experimental values and there is a systematic trend with increasing neutron number in which this difference decreases until at $N \geqslant 62$ it becomes close to zero, indicating good agreement between theory and experiment. The calculation for the Mo isotopes shows a small degree of odd-even staggering and places the Mo moments at similar values to the most-deformed Zr fragments, whereas in the data for the Mo isotopes $Q_{\rm DPM}$ reaches its maximum values in ^{105,107}Mo but is still lower than the value for ^{104}Zr [3.92(30)eb]. Similar to the Sr and Zr isotopes, the Ru isotopes show a trend of almost linearly decreasing difference between theory and experiment, this time from $N = 64$ to 67, until finally the agreement is close to the experimental error for ^{114,116}Pd. The most striking differences between the experiment and theory are in the Mo isotopes, i.e., the lower-than-expected quadrupole moments and the strong odd-even staggering, and in the rate of the onset of deformation in the Sr and Zr isotopes, which is more rapid in the experimental data than in the calculations. However, over the region as a whole, the agreement is reasonable, given that Q_0 represents the ground state and $Q_{\rm DPM}$ is measured at $I \sim 10$, and that the calculations are not particularly tuned to this mass region.

Reference [70] provides a a theoretical basis from which to study the effect of rotation in the $A \sim 100$ region by including a cranking term in the Woods-Saxon potential of a macroscopic/microscopic model. The authors present deformations for the minimum-energy solutions to the Hamiltonian and quadrupole moments for the proton distributions Q, for prolate and oblate, ground-state as well as excited-state configurations, as the relevant quantities to compare with data from lifetime measurements. Figure 7 shows a comparison of Q (for the ground state) with $Q_{\rm DPM}$, with the upper panel showing

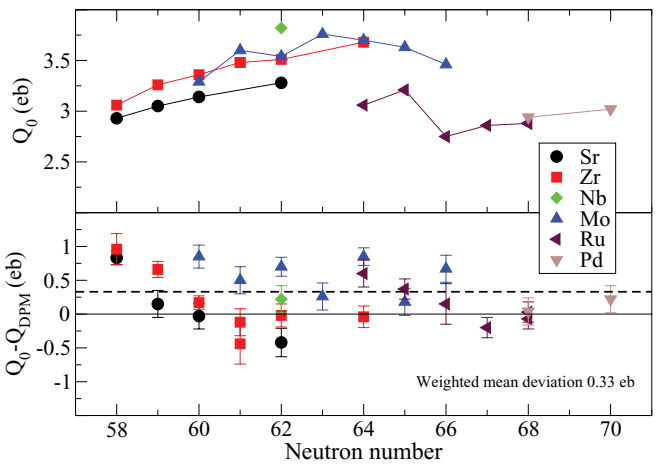

FIG. 6. (Color online) Comparison of the results of the DPM analysis with the calculations of Möller *et al.* [69].

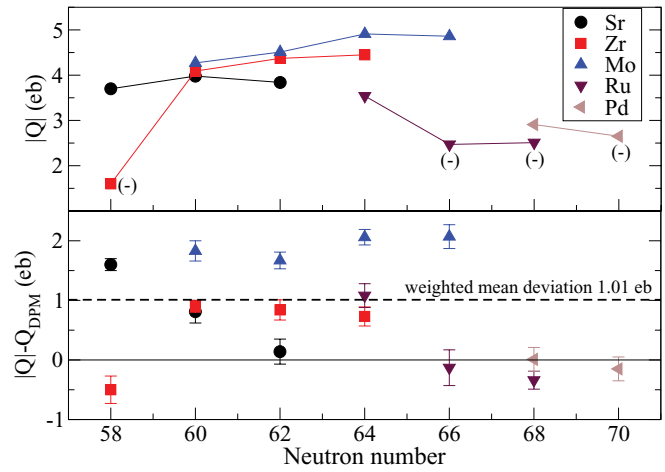

FIG. 7. (Color online) Transition quadrupole moments compared with the results of the calculations of Skalski *et al.* [70] for nuclear ground states. Oblate minimum-energy solutions have been indicated in the upper panel by the symbol (−), otherwise the solutions are prolate.

the calculations and the lower panel showing the difference between theory and experiment. These calculations only deal with even-even nuclei, but immediately some of the same discrepancies that appeared in the comparison with Ref. [69] are apparent; in an isotonic chain with $N > 59$ Q is largest for $_{42}$Mo whereas $Q_{\rm DPM}$ for the even-even Mo fragments is lower than those for $_{38}$Sr and $_{40}$Zr. As in Ref. [69], the onset of deformation in the Sr isotopes is significantly sharper in the data than in theory and theory generally overpredicts the magnitude of the quadrupole moments of the region (in this case the mean difference is 1.01 eb). The best agreement is found in ^{102}Zr, ^{110,112}Ru, and ^{114,116}Pd for which $Q_{\rm DPM}$ and Q are consistent to within experimental uncertainties. In Ref. [70], rotation of the nucleus up to $I \sim 10$ has very little effect on the predicted quadrupole moments of the Sr and Zr isotopes; the alignment of a pair of $h_{11/2}$ neutrons only serving to take the nucleus to slightly negative values of γ. The calculations for the Mo isotopes show potential-energy surfaces that are softer in γ but the minimum-energy configuration corresponds to slightly negative γ. In these calculations there is no shift in the deformation to positive γ with increasing rotation, and the prolate ground state becomes more secure with increasing neutron number. This is in contrast to the total Routhian surface calculations presented in an earlier work [19], which predicted a decrease in Q with increasing spin caused by a shift in the minimum to positive γ. The softness of the nucleus to γ deformation means that calculations are particularly challenging in the neutron-rich Mo isotopes; relatively small differences in the choice of model parameters result in either a prolate or an oblate configuration being labeled as yrast and thereby produce relatively large effects in the calculated value of Q. The authors of Ref. [70] suggest that the disagreement between their calculations and the experimental results for the even-even Mo isotopes may be due to a suppression in the value of $Q_{\rm DPM}$ in the region of the crossing between the ground-state and the two-quasiparticle band, due to band mixing over a small range in spin. It is difficult to further explore this possibility experimentally without the measurement of lifetimes above the band crossing region, where, if the explanation is correct, the Mo quadrupole moments should be seen to rise as the rotational frequency exceeds the crossing frequency.

Experimental evidence for changes in Q with spin may be examined through comparison of $Q_{\rm DPM}$ with the results of lifetime measurements at lower spin. Lifetime data have been measured for several even-even nuclei in the region, and Ref. [68] provides accepted values of the reduced transition probability $B(E2)\uparrow$, for the transition from the ground state to the first excited 2^+ state, and the equivalent intrinsic quadrupole moments at $I = 2$, which we refer to as Q_{2^+} (see Tables I–IV) . The ratio $R = Q_{\rm DPM}/Q_{2^+}$ is presented in Fig. 8 from which it is clear that for many of the nuclei in this survey R is significantly different from unity and therefore inconsistent with a picture of unvarying deformation with increasing spin. Using Fig. 8 as a guide, the data may be subdivided by atomic number into three groups and a weighted average of R taken in each group to obtain: for ^{96,98,100}Sr and ^{100,102}Zr, $\bar{R}_{\rm Sr,Zr} = 0.94 \pm 0.03$; for ^{102,104,106,108}Mo and ^{108,110,112}Ru, $\bar{R}_{\rm Mo,Ru} = 0.78 \pm 0.04$; and for the ^{114,116}Pd, $\bar{R}_{\rm Pd} = 1.26 \pm 0.15$. Taken at face value these results would suggest a small change in shape with rotation in the Sr and Zr isotopes, a larger and statistically more significant reduction in Q in the Mo and Ru isotopes and a hint of an increase in Q in ^{114,116}Pd. A caveat is that this analysis relies on a comparison of measurements performed using different experimental setups and techniques which may contain unaccounted systematic errors. For example, the DPM results rely on an assumed knowledge of the physical characteristics of the source and the stopping powers of the fragments within the KCl pellet (introducing an estimated systematic error of 5% in R), whereas the plunger and direct-timing techniques have their own particular sources of systematic error. In Ref. [73] lifetime measurements were made as a function of spin using a differential plunger in the nuclei ^{100}Zr and ^{104}Mo that showed that Q decreases by around 20% between $I = 4$ and $I = 8$ in the case of ^{104}Mo while remaining constant in ^{100}Zr, an observation that is consistent with the data presented in the present paper. Another way of looking at the DPM data that reduces the effect of systematic errors, is to take the Sr and Zr isotopes (theoretically the most rigid in shape) as a calibration of the technique. In this case there is a significant difference in the behavior with spin of the Mo and Ru isotopes to the nuclei used as calibration points. Furthermore, the odd-even staggering in Mo isotopes is an observation relatively insensitive to systematic errors in the technique. It should also be noted that the DPM measurements in ^{114,116}Pd lie above a pronounced backbend and that the observed increase in Q may well be associated with this sudden change in intrinsic structure; probably indicating the occupation of deformation-driving quasiparticle orbitals at the backbend.

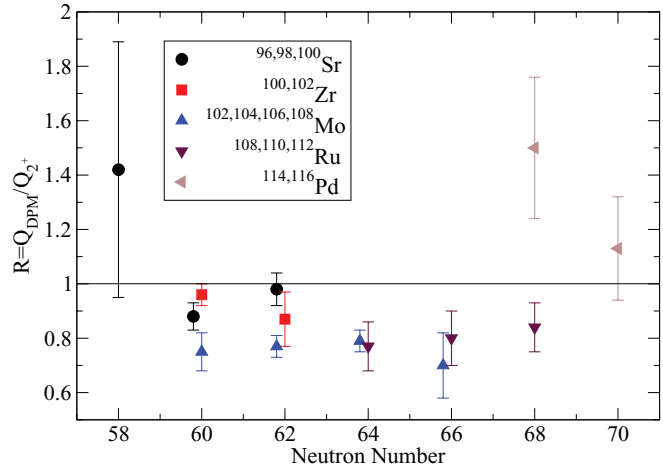

FIG. 8. (Color online) Ratio of $Q_{\rm DPM}$ to the evaluated experimental results of Q_{2^+} from Ref. [68].

In order to further elucidate the role of prolate-oblate competition and the γ degree of freedom in this mass region the proton quadrupole moments for both prolate and oblate energy minima have been extracted from self-consistent mean-field calculations [71,72]. These are shown in Fig. 9 where they are

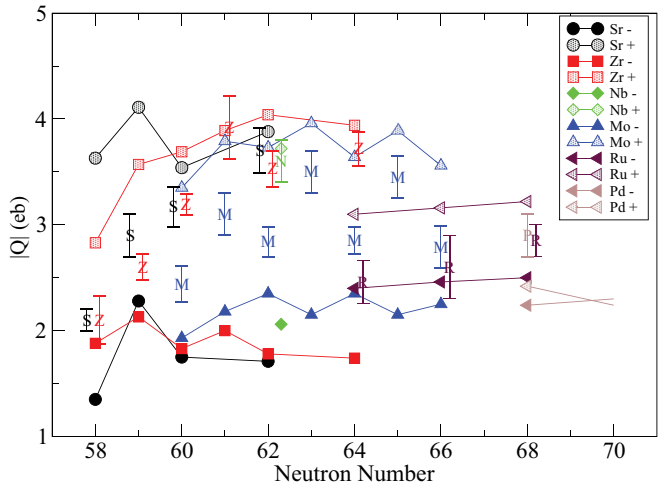

FIG. 9. (Color online) Quadrupole moments for proton distributions computed using the results of Refs. [71,72] (shown as geometric symbols) and compared with Q_{DPM}. Prolate minima are indicated as '+' and oblate as '−'. Abbreviated atomic symbols are used for the DPM data points, *viz*. S(Sr), Z(Zr), N(Nb), M(Mo), R(Ru), and P(Pd).

compared to the DPM data. In general the calculations reveal the prolate minima to have moments of approximately $Q \sim 3.5\,e$b, whereas the oblate minima are around $Q \sim -2\,e$b, with both minima showing some dependence on neutron number. In general, the prolate and oblate minima lie close in energy in the calculations. Within this picture, the Sr and Zr isotopes make a transition from oblate to prolate at $N \sim 59$. This transition is fairly smooth, implying a certain mixing between the two configurations. Such prolate-oblate mixing has been considered previously in ^{96}Sr and ^{98}Zr in complex excited VAMPIR calculations [74]. The maximum prolate deformations reached in the region are fully consistent with the calculations presented in Fig. 9 and correspond to $Q \sim 4\,e$b. ^{103}Nb is clearly prolate at $I \sim 10$. Interestingly, the Mo nuclei are not well reproduced by either the prolate or oblate extremes and there may be a subtle mix of the two configurations at play here; this might be expected, given the predicted triaxial softness of these nuclei. Figure 9 is suggestive that the even Mo isotopes are more oblate in nature and that the addition of an odd neutron favors the prolate configuration. This would be consistent with the occupation of the prolate-deformation-driving orbitals of $h_{11/2}$ parentage that are identified with the yrast sequences in these nuclei. The Ru isotopes appear to be oblate at $I \sim 10$ but in this case the odd neutron has less of an effect than in the Mo isotopes. In this picture there is a favoring of the oblate configuration with increasing Z. Consequently, one would expect the Pd isotopes to be oblate. However, ^{114,116}Pd have a higher than expected deformation at $I \sim 10$, greater than both the prolate and oblate predictions. This could indicate an increase of quadrupole moment with rotation as was suggested by the above comparison between Q_{2^+} and Q_{DPM}.

In summary, this paper has presented new lifetime measurements for excited rotational states in ^{101}Zr, ^{103}Nb, ^{108,109,110,111,112}Ru, and ^{114,116}Pd from which transition quadrupole moments at $I \sim 10$ have been extracted. The new results have been combined with the previously-published data from the same experiment to enable a study to be made of the evolution of nuclear shape. A comparison has been made with three different theoretical approaches. The results indicate several key features: that the onset of deformation in the Sr and Zr isotopes with N is relatively smooth at $I \sim 10$ and is probably a result of the mixing of prolate and oblate collective configurations; that the Sr and Zr isotopes have shapes that are reasonably unchanged by increasing the spin from $I = 2$ to $I = 10$, whereas the even-A Mo and the Ru isotopes show evidence of a decrease in quadrupole moment with increasing spin. This decrease is probably due to a shift from prolate to more oblate (triaxial) shapes, but a suppression of Q due to strong band mixing cannot be ruled out on the basis of the experimental evidence alone; that ^{103}Nb and the odd-A Mo isotopes are more prolate than oblate and that the odd neutron drives the shape towards prolate in the case of the odd-A Mo isotopes. The most challenging aspect for theory in this region appears to be a detailed reproduction of the behavior of the Mo and Ru isotopes where the balance between prolate and oblate configurations is at its most delicate and small changes to spin or particle number produce large changes to the transition quadrupole moments. There is clearly also a need for more extensive lifetime measurements, in particular using the plunger technique, which would enable Q to be mapped out as a function of I as well as Z and N.

ACKNOWLEDGMENTS

EUROGAM was funded jointly by IN2P3 (France) and the EPSRC (UK). This work was partly supported by the EPSRC under grant no. GRH71161 and by the the US Department of Energy, Office of Nuclear Physics, under contract no. DE-AC02-06CH11357. The authors are also indebted for the use of ^{248}Cm to the Office of Basic Energy Sciences, US Department of Energy, through the transplutonium element production facilities at the Oak Ridge National Laboratory. P.S. acknowledges support from MINECO (Spain) under Contract No. FIS2011-23565.

[1] A. Bohr and B. R. Mottelson, *Nuclear Structure* (Benjamin, New York, 1975).
[2] J. Wood, K. Heyde, W. Nazarewicz, M. Huyse, and P. van Duppen, Phys. Rep. **215**, 101 (1992).
[3] K. Heyde and J. L. Wood, Rev. Mod. Phys. **83**, 1467 (2011).
[4] E. Cheifetz, R. C. Jared, S. G. Thompson, and J. B. Wilhelmy, Phys. Rev. Lett. **25**, 38 (1970).
[5] M. A. C. Hotchkis *et al.*, Phys. Rev. Lett. **64**, 3123 (1990).
[6] M. A. C. Hotchkis *et al.*, Nucl. Phys. A **530**, 111 (1991).
[7] A. Guessous *et al.*, Phys. Rev. Lett. **75**, 2280 (1995).
[8] J. A. Shannon *et al.*, Phys. Lett. B **336**, 136 (1994).
[9] C. Y. Wu *et al.*, Phys. Rev. C **73**, 034312 (2006).
[10] S. J. Zhu *et al.*, Int. J. Mod. Phys. E **18**, 1717 (2009).
[11] J. A. Pinston *et al.*, Phys. Rev. C **74**, 064304 (2006).

[12] R. Orlandi *et al.*, Phys. Rev. C **73**, 054310 (2006).
[13] W. Urban *et al.*, Eur. Phys. J. A **20**, 381 (2004).
[14] H. Watanabe *et al.*, Phys. Lett. B **704**, 270 (2011).
[15] W. Urban, T. Rzaca-Urban, J. L. Durell, A. G. Smith, and I. Ahmad, Eur. Phys. J. A **24**, 161 (2005).
[16] J. Kurpeta *et al.*, Phys. Rev. C **84**, 044304 (2011).
[17] H. Watanabe *et al.*, Phys. Lett. B **696**, 186 (2011).
[18] A. G. Smith *et al.*, Phys. Rev. Lett. **73**, 2540 (1994).
[19] A. G. Smith *et al.*, Phys. Rev. Lett. **77**, 1711 (1996).
[20] W. Urban *et al.*, Nucl. Phys. A **689**, 605 (2001).
[21] P. J. Nolan, F. A. Beck, and D. B. Fossan, Annu. Rev. Nucl. Part. Sci. **44**, 561 (1994) http://www.annualreviews.org/doi/pdf/10.1146/annurev.ns.44.120194.003021.
[22] A. G. Smith, Nucl. Instrum. Methods Phys. Res. A **381**, 517 (1996).
[23] J. Ziegler, J. Biersack, and U. Littmark, *The Stopping and Range of Ions in Solids* (Pergamon Press, New York, 1985).
[24] V. E. Viola, K. Kwiatkowski, and M. Walker, Phys. Rev. C **31**, 1550 (1985).
[25] S. L. Whetstone, Phys. Rev. **131**, 1232 (1963).
[26] B. Singh and Z. Hu, Nucl. Data Sheets **98**, 335 (2003).
[27] E. Browne and J. K. Tuli, Nucl. Data Sheets **112**, 275 (2011).
[28] B. Singh, Nucl. Data Sheets **109**, 297 (2008).
[29] J. Blachot, Nucl. Data Sheets **83**, 1 (1998).
[30] D. De Frenne, Nucl. Data Sheets **110**, 1745 (2009).
[31] J. Blachot, Nucl. Data Sheets **108**, 2035 (2007).
[32] D. De Frenne and E. Jacobs, Nucl. Data Sheets **105**, 775 (2005).
[33] D. De Frenne and A. Negret, Nucl. Data Sheets **109**, 943 (2008).
[34] J. Blachot, Nucl. Data Sheets **109**, 1383 (2008).
[35] J. Blachot, Nucl. Data Sheets **91**, 135 (2000).
[36] J. Blachot, Nucl. Data Sheets **107**, 355 (2006).
[37] D. De Frenne and E. Jacobs, Nucl. Data Sheets **89**, 481 (2000).
[38] J. Blachot, Nucl. Data Sheets **110**, 1239 (2009).
[39] D. De Frenne and E. Jacobs, Nucl. Data Sheets **79**, 639 (1996).
[40] J. Blachot, Nucl. Data Sheets **97**, 593 (2002).
[41] J. Blachot, Nucl. Data Sheets **111**, 717 (2010).
[42] W. Urban *et al.*, Eur. Phys. J. A **22**, 241 (2004).
[43] J. K. Hwang *et al.*, Phys. Rev. C **58**, 3252 (1998).
[44] H. Hua *et al.*, Phys. Rev. C **65**, 064325 (2002).
[45] J. A. Pinston *et al.*, Phys. Rev. C **74**, 064304 (2006).
[46] H. B. Ding *et al.*, Phys. Rev. C **74**, 054301 (2006).
[47] M. Liang, H. Ohm, B. De Sutter, and K. Sistemich, Z. Phys. A **344**, 357 (1993).
[48] J. K. Hwang *et al.*, J. Phys. G (London) **24**, L9 (1998).
[49] H. Hua *et al.*, Phys. Rev. C **69**, 014317 (2004).
[50] M. Liang, H. Ohm, B. De Sutter-Pomme, and K. Sistemich, Z. Phys. A **351**, 13 (1995).
[51] H. G. Borner *et al.*, Nucl. Instrum. Methods **164**, 579 (1979).
[52] W. Urban *et al.*, Phys. Rev. C **72**, 027302 (2005).
[53] J. Stachel *et al.*, Z. Phys. A **316**, 105 (1984).
[54] Q. H. Lu *et al.*, Phys. Rev. C **52**, 1348 (1995).
[55] I. Deloncle *et al.*, Eur. Phys. J. A **8**, 177 (2000).
[56] M. Graefenstedt *et al.*, Z. Phys. A **334**, 239 (1989).
[57] J. K. Hwang *et al.*, J. Phys. G (London) **24**, L9 (1998).
[58] F. F. Hopkins, J. R. White, C. F. Moore, and P. Richard, Phys. Rev. C **8**, 380 (1973).
[59] K. Butler-Moore *et al.*, Phys. Rev. C **52**, 1339 (1995).
[60] J. Aysto *et al.*, Nucl. Phys. A **515**, 365 (1990).
[61] Y. X. Luo *et al.*, Int. J. Mod. Phys. E **18**, 1697 (2009).
[62] B. Pfeiffer *et al.*, Eur. Phys. J. A **2**, 17 (1998).
[63] W. Urban *et al.*, Eur. Phys. J. A **22**, 231 (2004).
[64] J. Aysto *et al.*, Nucl. Phys. A **480**, 104 (1988).
[65] K. Butler-Moore *et al.*, J. Phys. G (London) **25**, 2253 (1999).
[66] Y. Wang *et al.*, Phys. Rev. C **63**, 024309 (2001).
[67] J. L. Durell, Fission Fragment Spectroscopy, in Proceedings of the International Conference on Spectroscopy of Heavy Nuclei, 1990.
[68] S. Raman, C. Nestor Jr., and P. Tikkanen, At. Data Nucl. Data Tables **78**, 1 (2001).
[69] P. Moller, J. Nix, W. Myers, and W. Swiatecki, At. Data Nucl. Data Tables **59**, 185 (1995).
[70] J. Skalski, S. Mizutori, and W. Nazarewicz, Nucl. Phys. A **617**, 282 (1997).
[71] R. Rodriguez-Guzman, P. Sarriguren, L. M. Robledo, and S. Perez-Martin, Phys. Lett. B **691**, 202 (2010).
[72] R. Rodriguez-Guzman, P. Sarriguren, and L. M. Robledo, Phys. Rev. C **83**, 044307 (2011).
[73] A. G. Smith *et al.*, J. Phys. G (London) **28**, 2307 (2002).
[74] A. Petrovici, Phys. Rev. C **85**, 034337 (2012).